AD-A063 521 ARMY ARMAMENT RESEARCH AND DEVELOPMENT COMMAND ABERD--ETC F/G 19/1
REPLICA MODELING OF THE LAUNCH AND FLIGHT DYNAMICS OF PROJECTIL--ETC(U)
SEP 78 E M SCHMIDT, B P BURNS, G SAMOS

UNCLASSIFIED ARBRL-TR-02104 SBIE-AD-E430 163 NL

1 OF
AD
AD63 521

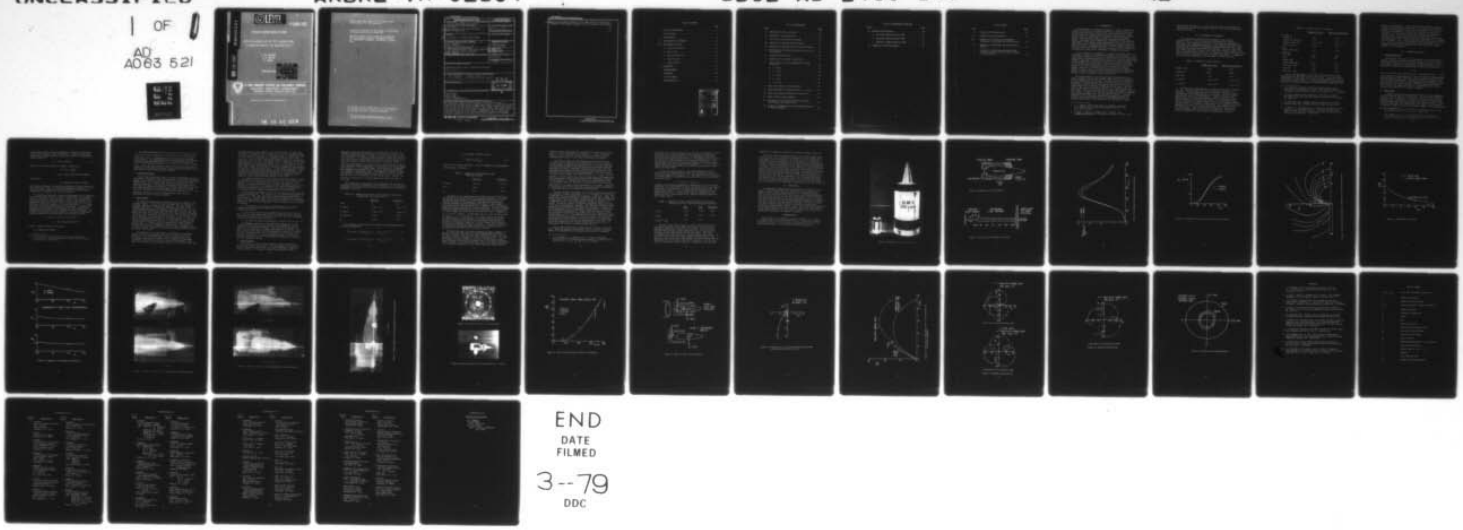

END
DATE
FILMED
3--79
DDC

AD A063521

DDC FILE COPY

(12) LEVEL II

AD-E430 163

TECHNICAL REPORT ARBRL-TR-02104

REPLICA MODELING OF THE LAUNCH AND FLIGHT DYNAMICS OF PROJECTILES

E. M. Schmidt
B. P. Burns
G. Samos

September 1978

DDC
RECEIVED
JAN 22 1979
B

US ARMY ARMAMENT RESEARCH AND DEVELOPMENT COMMAND
BALLISTIC RESEARCH LABORATORY
ABERDEEN PROVING GROUND, MARYLAND

Approved for public release; distribution unlimited.

78 12 12 228

Destroy this report when it is no longer needed.
Do not return it to the originator.

Secondary distribution of this report by originating or sponsoring activity is prohibited.

Additional copies of this report may be obtained from the National Technical Information Service, U.S. Department of Commerce, Springfield, Virginia 22161.

The findings in this report are not to be construed as an official Department of the Army position, unless so designated by other authorized documents.

The use of trade names or manufacturers' names in this report does not constitute indorsement of any commercial product.

UNCLASSIFIED

SECURITY CLASSIFICATION OF THIS PAGE (When Data Entered)

REPORT DOCUMENTATION PAGE

READ INSTRUCTIONS BEFORE COMPLETING FORM

1. REPORT NUMBER: TECHNICAL REPORT ARBRL-TR-02104

2. GOVT ACCESSION NO.

3. RECIPIENT'S CATALOG NUMBER

4. TITLE (and Subtitle): REPLICA MODELING OF THE LAUNCH AND FLIGHT DYNAMICS OF PROJECTILES.

5. TYPE OF REPORT & PERIOD COVERED: Final rept.

6. PERFORMING ORG. REPORT NUMBER

7. AUTHOR(s): E. M. Schmidt, B. P. Burns, and G. Samos

8. CONTRACT OR GRANT NUMBER(s)

9. PERFORMING ORGANIZATION NAME AND ADDRESS
US Army Ballistic Research Laboratory
(ATTN: DRDAR-BLL)
Aberdeen Proving Ground, MD 21005

10. PROGRAM ELEMENT, PROJECT, TASK AREA & WORK UNIT NUMBERS
RDT&E 1L162618AH80

11. CONTROLLING OFFICE NAME AND ADDRESS
US Army Armament Research & Development Command
US Army Ballistic Research Laboratory
(ATTN: DRDAR-BL)
Aberdeen Proving Ground, MD 21005

12. REPORT DATE: SEPTEMBER 1978

13. NUMBER OF PAGES: 47

14. MONITORING AGENCY NAME & ADDRESS (if different from Controlling Office)

15. SECURITY CLASS. (of this report): Unclassified

15a. DECLASSIFICATION/DOWNGRADING SCHEDULE

16. DISTRIBUTION STATEMENT (of this Report)

Approved for public release; distribution unlimited.

45 p.

17. DISTRIBUTION STATEMENT (of the abstract entered in Block 20, if different from Report)

SBIE AD-E430 163

DDC
RECEIVED
JAN 22 1979
B

18. SUPPLEMENTARY NOTES

19. KEY WORDS (Continue on reverse side if necessary and identify by block number)

Sabot Discard
Muzzle Blast
Replica Modeling
Kinetic Energy Ammunition

20. ABSTRACT (Continue on reverse side if necessary and identify by block number) (ner)

An experimental program has been conducted to determine the limits of applicability of replica model scaling of gun systems. A one-third scale model of the 105mm, M68 tank gun and the M392 kinetic energy projectile are tested. Data are taken on the interior ballistics, muzzle blast, sabot discard dynamics, and exterior ballistics of the model. Comparison of the test results with available information on the full scale system shows that, as anticipated, accurate reproduction of the interior and exterior ballistics is achieved;

DD FORM 1 JAN 73 1473 EDITION OF 1 NOV 65 IS OBSOLETE

393 471

UNCLASSIFIED

SECURITY CLASSIFICATION OF THIS PAGE (When Data Entered)

however, while gross similarity in the sabot discard is observed, the magnitude of the launch disturbance in the two systems is not identical.

TABLE OF CONTENTS

ACCESSION for
NTIS White Section
DDC Buff Section
UNANNOUNCED
JUSTIFICATION
BY
DISTRIBUTION/AVAILABILITY CODES
Dist. SPECIAL
A

LIST OF ILLUSTRATIONS

LIST OF ILLUSTRATIONS (Continued)

LIST OF TABLES

I. INTRODUCTION

Gun performance is continually improved in order to maintain a competitive posture on the modern battlefield. Higher muzzle velocities increase lethality, extend range, and reduce time of flight. Advanced projectile shapes improve stability, reduce drag, increase payload, and ease automation. New propellants increase specific energy, reduce erosion, decrease flash, and improve combustion. However, overriding these technological innovations is the essential requirement of hitting the target, preferably on the first shot. To prove that a new or improved gun system maintains specified accuracy, the Army invests considerable resources in field testing. Often the full scale data are limited, providing indication of the existence of a problem but giving little information to diagnose the origin.

It is of interest to determine if a portion of the full-scale development testing can be replaced by reduced scale experiments. This would permit savings on facilities and equipment costs while providing a more benign environment favorable to the installation of sophisticated diagnostic equipment. Reduced scale testing is a common procedure. An obvious example being wind tunnel testing of aircraft and missiles. In ballistics, this type testing is well established in the determination of projectile aeroballistics[1] and in charge development[2]; however, data are not available describing the scaling of launch dynamics, which is taken to include perturbations to the projectile's nominal or desired trajectory due to in-bore vibrations, transit of the muzzle blast, and sabot discard interactions.

This paper addresses replica modeling of the performance of a kinetic energy projectile for the M68, 105mm gun which is currently the main armament of the M60 tank. The M392, sabot, spin-stabilized projectile is considered both because of the restrictive accuracy requirement placed on direct fire tank gun ammunition and because of recent launch related problems experienced by the round. Data are taken on the interior ballistics, muzzle blast, sabot discard, and free flight motion of the one-third scale model and compared with full-scale tests. An analysis of the sabot discard mechanisms is presented which agrees reasonably well with the measured results. From measurements taken of the sabot and projectile dynamics during the discard process coupled with ballistic range measurements of the initial yawing motion of the projectile, the existence of strong

---

1. *C. H. Murphy, "Free Flight Motion of Symmetric Missiles," U. S. Army Ballistic Research Laboratory Report No. 1216, July 1963, AD 442757.*

2. *F. Hunt, G. Hinds, C. Clemmow, and C. Tranter, (ed), Internal Ballistics, The Philosophical Library, New York, 1951.*

sabot discard interactions is established and shown to be dependent on the magnitude of transverse angular velocity of the round at separation from the gun tube.

II. TEST MODELS AND APPARATUS

The reduced-scale and full-scale projectiles are shown in Figures 1a and 1b. The two rounds were fabricated from identical materials. The sub-projectiles consist of high density tungsten and steel penetrator components encased in a steel and aluminum outer sheath. The sabots are fabricated from magnesium and aluminum alloys with nylon centering bands and pressed fiber rotating bands. The full-scale round has a rubber obturator; however, this could not be readily formed in the smaller dimensions and was deleted. No significant blow-by was experienced due to the lack of obturation of the one-third scale model. A comparison of the inertial properties of the two rounds is given in Table I.

TABLE I. Properties of Sub-projectile

	105mm (full-scale)	35mm (one third-scale)
Diameter (mm)	60.91	20.31
Length (mm)	264.92	88.75
Mass (kg)	4.04	0.149
K_x (kg-m^2)	1.16×10^{-3}	4.78×10^{-6}
I_y (kg-m^2)	1.09×10^{-2}	4.48×10^{-5}

The 35mm gun was manufactured to scaled specifications of the M68 tank gun. The tube length and twist of rifling (in calibers) were replicated. The rifling design was also matched. However, since an existing 40mm breech mechanism had to be utilized, the exact chamber configuration could not be maintained. A 40mm, M25 case was cut down to mate with a titanium dioxide/wax liner (simulating the wear reducing additive of the full-scale round). This configuration produced a scaling of the chamber volume, but not of the chamber geometry. The propellant was specifically manufactured to the composition and scale geometry of the full size, seven perforation, M30 propellant used in the M68 tank gun. Due to manufacturing difficulties, some of the propellant grain dimensions could not be maintained. The interior ballistic parameters of both systems are summarized in Table II.

TABLE II. Interior Ballistic Parameters

	105mm (full scale)	35mm (one third-scale)
Gun Tube		
Length (m)	5.33	1.74
Projectile travel (m)	4.76	1.57
Chamber volume (m^3)	6.60×10^{-3}	2.43×10^{-4}
Twist (rev/cal)	1/18	1/18
Round		
In-bore mass (kg)	5.79	0.215
Propellant		
Mass (kg)	5.48	0.205
Type	M30	M30
Number perf.	7	7
Grain length (mm)	15.93	5.25
Grain dia. (mm)	6.63	2.40
Web (mm)	1.16	0.37
Perf. dia. (mm)	0.66	0.31

Data on the performance of the 105mm, M68 tank gun firing the M392 projectile comes from a variety of sources[3-5]. The one third-scale model was the subject of a series of tests conducted in the BRL Aeroballistics Range, Figure 2. In-bore measurements of pressure and projectile velocity were acquired[6] using BRL Minihat transducers and

---

3. *J. M. Frankle, "Interior Ballistics of High-Velocity Guns, Experimental Program-Phase 1," BRL MR 1879, Ballistic Research Laboratory, Aberdeen Proving Ground, MD, November 1967. AD 830408.*

4. *E. Kelly, "Firing Record: Cartridge, 105mm, APDS-T, M392A2," FR P-82598, Test and Evaluation Command, Aberdeen Proving Ground, MD, June 1977.*

5. *M. Piddington and F. Brandon, Private Communication, Ballistic Research Laboratory, Aberdeen Proving Ground, MD, April 1978.*

6. *G. Samos, B. B. Grollman, and J. Q. Schmidt, "Initial Firing Test Results of the 35mm Scaled Model of the 105mm M68 Tank Gun," ARBRL MR 02804, Ballistic Research Laboratory, Aberdeen Proving Ground, MD, January 1978. AD A051050.*

microwave interferometry. Muzzle blast was measured both optically and with side-on pressure transducers. Sabot discard and projectile dynamics were observed at a series of six orthogonal X-ray stations placed at 0.46m intervals over the first 2.38m of the projectile trajectory. The projectile entered the Aeroballistics Range after 3.4m of flight. Its free flight motion was measured using 25 orthogonal spark shadowgraph stations positioned over the remaining 95m of the trajectory. Discussion of these experiments will be broken into two phases. First, the measurements which were expected to scale, i.e., interior ballistics, muzzle blast, and aerodynamics, will be presented. Second, the measurements of sabot discard and launch dynamics will be examined.

III. EXPERIMENTAL RESULTS

A. Interior Ballistics

Hunt[2] defines the type of scaling applied in the current tests as Geometric Similarity and notes that the projectile velocity versus travel and pressurization versus travel histories will be identical in each weapon if the travel is expressed in terms of calibers. This is equivalent to defining a reference time according to the relation:

$$\tau = D/V_m \qquad (1)$$

where D is the gun tube diameter and V_m is the launch velocity. Using this parameter to nondimensionalize time, the measured chamber pressure and projectile velocity variations, Figure 3a and 3b, are similar for both the 105mm and 35mm guns. The minor differences between the two sets of data are ascribed to the discrepancies in the chamber configurations and lack of exact scaling of the propellant grain geometry. Hunt[2] reports that during World War II, Krupp applied this type of scaling to design guns up to 800mm in diameter.

B. Muzzle Blast

A number of attempts have been made to develop scaling parameters which describe the muzzle blast from guns. One of the most extensive studies is that of Westine[7]. He presents a universal blast scaling relation which is supposedly valid for a wide variety of guns having differing geometries, projectile masses, and launch velocities. While there are some data[8] which suggest that the extent of the scaling may be limited in terms of variety of different weapons, it is probable that

7. *P. S. Westine, "The Blast Field About the Muzzle of Guns," Shock and Vibration Bulletin, No. 39, Pt. 6, March 1969.*

8. *E. M. Schmidt and E. J. Gion, "Muzzle Blast of 30mm Cannon," ARBRL-MR-02805, Ballistic Research Laboratory, Aberdeen Proving Ground, MD, January 1978. AD B024973L.*

the scaling relations should be applicable to affinely related guns such as those presently under consideration. Westine indicates for geometrically similar locations in the blast field, the overpressures scale according to

$$(p - p_\infty)/P_\infty = f(W/D^2L), \qquad (2)$$

where D,L = gun tube diameter and length, respectively,

$$W = m_c e_c - m_p V_m^2/2,$$

m_c, m_p = charge and projectile masses,

respectively,

e_c = propellant specific energy.

The 105mm and 35mm guns use identical propellant and launch rounds with equal velocities. Thus, the functional parameter in Equation (2) is the same for both weapons, and the blast fields should have equal overpressures at geometrically similar locations.

In the present experiment, extensive measurements of the free field blast were obtained, Figure 4; however, similar data is not currently available for the full scale tank gun. The only blast record which could be uncovered for the 105mm gun was taken at the location of the commander's cupola on the tank. This is located along the 150° ray from the line of fire a distance of 55D from the muzzle, i.e., beyond the range of the measurements taken on the 35mm gun. To extend the 105mm data into the area of the present tests, use is made of the Whitham far field scaling law as presented by Ranlet and Erdos[9]. They indicate that asymptotic analysis predicts a far field overpressure decay for spherical waves according to the following relation:

$$(p - p_\infty)/p_\infty = 0.472\ (\gamma/[\gamma+1])(r/r_o)^{-1}$$

$$(\ln[0.425 r_o/D]/\ln[r/D])^{1/2} \qquad (3)$$

where r = radial location of blast wave

r_o = energy scale radius.

---

9. *J. Ranlet and J. Erdos, "Muzzle Blast Field Calculations," CR 297, Ballistic Research Laboratory, Aberdeen Proving Ground, MD, April 1976. AD B011967L.*

The 105mm measurements give: at r/D = 55.5, $(p - p_\infty)/p_\infty = 0.056$. Using these values to define r_o/D in Equation (3), the overpressure relation may then be extrapolated back into the range of the 35mm data, Figure 5. The agreement between the 35mm measured overpressures and the extrapolated 105mm datum is quite good over the region of validity of the Whitham relation (i.e., until $M_s = 1.1$ or $[p - p_\infty]/p_\infty = 0.245$). While the blast pressures should scale and the data indicate reasonable verification of this fact, more detailed measurements in the blast field of the full-scale gun are required.

C. Exterior Ballistics

The similarity laws which apply to inviscid aerodynamics are well established. For geometrically related shapes, the pressure distribution around the two bodies is equivalent if they are moving at the same Mach number relative to the fluid. The 35mm and 105mm projectiles have identical geometries. The measured aerodynamic coefficients for the two rounds are summarized in Figure 6. Data have been obtained for the full scale round over a wide Mach number range[5]; however, the 35mm projectile was fired at only one (midrange) Mach number, $M_\infty = 4.0$. The comparison between the two sets of measurements shows that the anticipated inviscid scaling is achieved.

D. Sabot Discard

The sabot discard process was measured using the orthogonal X-ray stations, Figure 7. Only five X-rays are shown due to a failure of the final station to trigger in this sequence. The sabot discard is somewhat complicated. At separation from the muzzle, the nylon centering band fails and is discarded by centrifugal action. The sabot petals break the narrow shear ring connecting them with the sabot cup under the action of set-back within the tube. When the nylon centering band fails, they are free to fly off as is seen in the first two X-rays of the sequence. Upon penetration of the muzzle blast, the sabot cup begins to decelerate with respect to the flight body due to the drag and mass differences between the two. As the sabot cup and the projectile move down range, a relative yawing motion becomes apparent between them. At 1.47m, mechanical contact occurs. The details of the sabot discard will be addressed in the following paragraphs, and the effect of sabot discard on the projectile launch dynamics discussed in the next sub-section.

The separation of the sabot petals is dominated by centrifugal effects and is quite repeatable from round-to-round for the 35mm projectile. The sabot petal impacts onto a witness board placed 3.2m from the gun muzzle, Figure 8, for five separate firings form a concentric circle about the central projectile passageway. Also shown on the figure are the predicted impact circle (for both the 105mm

and 35mm) and the actual impact circle[4] for the 105mm. The prediction is based on a calculation of the tangential velocity of the petal center of gravity due to launch spin. For the 35mm round, the launch spin rate is 2.24×10^3 rev/s resulting in a tangential velocity of the sabot petal c.g. of 155 m/s, or an equivalent departure angle of 6.26^o against a measured value of 5.88^o. An identical value is predicted for the 105mm round; however, the actual measurements is 2.8^o. The reason for this poor correlation is the behavior of the nylon centering band of the full scale round. Rather than failing at the muzzle immediately upon release, the full-scale band can remain intact. In the smear photograph of Figure 9, the band is observed on the forward portion of the projectile. The integrity of the band retards free separation of the sabot petals and points out that failure mechanisms are not always reproduced in the simplistic replica modeling being examined in this paper.

An alternate hypothesis for the failure of the sabot petals to scale can be offered. The petals are freed from the rest of the sabot by the fracture of a shear web caused by axial in-bore acceleration. The angular in-bore acceleration history, and hence the angular velocity of the petals at shot exit is influenced by the fracture characteristics and friction between the tube, the sabot body, and the subprojectile. It is possible that this complicated phenomena was not duplicated.

The rearward displacement of the sabot cup relative to the projectile is plotted in Figure 10. The ordinate, ΔZ, is the difference between the measured c.g. of the sabot cup and its assembled position relative to the projectile. The 35mm sabot cup falls back somewhat faster than does that of the 105mm round. Again this reflects the effect of the differing behavior of the nylon centering bands. The calculated curve is obtained by assuming

1. the pressure on the sabot cup leading edge is equal to the stagnation pressure behind a normal shock in air with $M_\infty = 4.21$ (launch Mach number);

2. the cavity pressure is the stagnation pressure until the exit hole in the cup base opens sufficiently to unchoke the annulus between the sabot wall and the projectile body (after this the flow is computed using quasi-one-dimensional theory); and

3. the sabot and projectile penetrate the muzzle blast at $Z/D = 10$.

The agreement between the calculated and measured data is good indicating that the gross discard dynamics and aerodynamics can be treated in a straightforward manner. The yawing motion between the sabot cup and flight body is somewhat more difficult to handle. This is due in part to the complexity of the aerodynamics necessary to describe the three dimensional flow, but more importantly, the relative yaw is strongly influenced by the initial separation dynamics of the round. These are determined by the in-bore mechanical interactions which have yet to be adequately defined.

E. Launch Dynamics

The relative yaw and eventual mechanical contact between the sabot cup and flight body, Figure 7, may be explained by considering both the separation dynamics and free flight aerodynamic properties of the two bodies. Two phases of discard are proposed, Figure 11.

Immediately upon leaving the muzzle, the sabot petals separate, but the sabot cup and projectile are held in contact by the thrust of the exhausting propellant gases. During this initial phase, the two move as a rigid body. If transverse linear velocity is neglected, both the sabot and projectile rotate about their mutual center of gravity at a transverse angular velocity which is equal to the launch value, ξ_o'. This type motion results in a linear velocity of the center of gravity of the separate bodies in proportion to the angular rate and the moment arms, Figure 11. In the second phase, the two bodies are independent. This commences upon penetration of the muzzle blast when the bodies are separated by aerodynamic loads. The momentum is conserved during the separation, and each body now rotates about its own c.g. at the angular rate, ξ_o', and translates at the velocity $\Delta_i\xi_o'$. However, the two linear velocities are in direct opposition which could lead to collision.

The possibility of collision would be reduced if the two bodies continued to rotate in coordination. The differences in the free flight aerodynamics of the projectile and sabot cup prevent this advantageous occurrence, Table III.

TABLE III. Comparison of Inertial and Aerodynamic Properties of 35mm Sabot Cup and Projectile

	Sabot Cup	Projectile
ℓ (mm)	35	20.3
I_x (kg-m^2)	0.99×10^{-5}	0.478×10^{-5}
I_y (kg-m^2)	0.985×10^{-5}	4.480×10^{-5}
ϕ_o' (rad/cal)	0.349	0.199
C_{m_α}	9.533	1.84

The influence on the motion of the bodies can be determined from the following equations[1]:

$$|\xi_{1st\ max}| = |\xi_o'|/([I_x\phi_o'/I_y]^2 - [\pi\rho\ell^5 C_{m_\alpha}/2I_y])^{1/2}, \quad (4)$$

$$T = \text{yaw period} = 2\pi\ell/([I_x\phi_o'/I_y]^2 - [\pi\rho\ell^5 C_{m_\alpha}/2I_y])^{1/2}, \quad (5)$$

$$s_g = \text{gyroscopic stability factor}$$

$$= 2I_x^2 \Phi_o'^2 / (\pi \rho \ell^5 C_{m_\alpha} I_y) \quad , \tag{6}$$

where Φ_o' is the launch spin rate. Table IV summarizes these parameters for the bodies of interest.

TABLE IV. Comparison of 35mm Sabot Cup and Projectile Motions

	Sabot Cup	Projectile
$\xi_{1st\ max}$	2.91 ξ_o'	74.2 ξ_o'
T (m)	0.64	9.5
s_g	22.8	1.68

The sabot cup is significantly more stable than is the projectile, and the motion of the two bodies is considerably different. The sabot cup performs high frequency, low amplitude oscillations; while the projectile engages in low frequency, large amplitude oscillations. From the postulated separation dynamics of Figure 11 and the above description of the free body motion, it is apparent that a sufficiently high launch angular velocity will produce collision. From the clearances between the sabot and projectile for the 35mm round, the limiting value of launch angular rate above which collision must occur is computed as $\xi_o' = 1.58 \times 10^{-3}$ rad/cal. The measured value of ξ_o' for the round shown in Figure 7 is 1.9×10^{-3} rad/cal. This value is above the minimum, and the calculated collision point is 1.58m from the weapon muzzle. The actual collision point can be best determined from measured yaw histories of the bodies, Figure 12. This plot shows the variation in the projectile and sabot cup angle of attack, α, and angle of sideslip, β, as they move through the X-ray field of view. Each data point corresponds to one of the first five X-ray stations.

The projectile shows no distinct response to impact; however, the motion of the lower mass sabot cup clearly demonstrates its effect. The sabot initially leaves the gun with a magnitude of angle of attack and yawing velocity coincident with those of the projectile. The large differences in dynamic properties, Table IV, between the two causes rapid divergence in this initial angular motion. The sabot cup reaches a first maximum of yaw between the first and second stations after which its yaw begins to diminish. At the third station the yawing velocity

suddenly reverses indicating the occurrence of a collision near this point Z = 1.01m (compared with a predicted Z = 1.58m). From examination of the X-rays, the contact appears to be maintained once established and the yaw of the sabot cup continues to diverge.

The effect of sabot discard interaction on the motion of the projectile can be observed in the measurements of its yaw, Figure 13. In this figure the magnitude of projectile yaw as it moves downrange is plotted from measured X-ray and Aeroballistic Range data and compared with the ideal, interference free trajectory. The X-ray data and Aeroballistic Range data (which have been extrapolated back into the region of X-ray data) are in good agreement at the point in the trajectory where complete sabot discard occurs, i.e., Z_{free}. However, neither set of data agrees well with the interference free computation. This calculation is made using the free flight aerodynamic properties of the projectile in conjunction with the X-ray measurements of the initial angular rate, ξ_o', and shows the yawing motion the projectile could follow if no sabot discard interference were present. Comparison of the three sets of curves indicates that sabot discard interference is significant and acts to amplify the yawing motion.

The sabot discard interference can be further explored by examining the variation in complex yaw angle, $\xi = \beta + i\alpha$, Figure 14. Three sets of measured data are presented for comparison: a full-bore, 175mm, spin-stabilized projectile; the 35mm, sub-caliber, round; and the 105mm, sub-caliber round. The motion shown in these figures is typical of that of a symmetric missile[1], and is described as two arm or epicyclic in nature. One arm is the fast or nutational component, while the other is the slow or precessional component. The arms sum according to their magnitude and orientation as the round moves downrange. Variations in the pattern occur as the arm magnitudes change relative to each other due to different damping rates. However, near the muzzle of a gun, the arms should be of nearly equal magnitude if the in-bore yaw level (approximately 0.2^o) is to be matched as an initial condition of launch. For the full-bore case, Figure 14a, this does occur. The full-bore round separates from the muzzle at the low in-bore level, penetrates the muzzle blast with little if any amplification in yaw rate[10], and enters free flight with the epicycle having nearly equal arms (as indicated by the continual cycling through zero yaw).

For the sabot projectiles, Figures 14b and 14c, this is not the case. When they separate from the gun, they fly through a disturbed region of considerable extent during which the sabot is discarded.

---

10. E. M. Schmidt, K. S. Fansler, and D. D. Shear, "Trajectory Perturbations of Fin-Stabilized Projectiles due to Muzzle Blast," AIAA, JSR, Vol. 14, No. 6, June 1977, pp. 339-344.

The influence of discard loadings causes the relative magnitude of the nutational and precessional arms to vary producing the open-center of the epicycles in the yawing plots. One additional observation should be made regarding these two plots. The magnitude of the angles are typical of those obtained for the 35mm and 105mm firings. The maximum angle of attack attained by the 35mm projectiles were consistently higher than that of the 105mm projectiles. It is of interest to examine the correlations which can be obtained from the mean yawing motions of these rounds.

For the full-bore projectile, since the minimum yaw level is nearly zero, the maximum angle of attack can be directly related to the launch angular rate, Equation (4). This angular rate is equivalent to the total impulse transferred to the projectile in-bore and through the muzzle blast:

$$\dot{\xi}_o = \int M/I_y \, dt = (V_m/D) \quad \xi'_o \tag{7}$$

Assuming this functional dependence is applicable to the sub-caliber projectile, the maximum angle of attack is related to the total impulse transferred to the projectile in-bore, through the muzzle blast, and during sabot discard. If it is assumed that the minimum yaw level, Figures 14b and 14c, is related to the impulse transferred to the projectile due to sabot discard alone, then the following comparison may be made, Table V.

TABLE V. Comparison of Mean Yawing Parameters from 10 Round Firings of the Full- and One Third-Scale Projectiles

	105mm	35mm	35mm/105mm
$\lvert\xi_{min}\rvert$	0.83^o	2.41^o	2.90
$\lvert\xi_{max}\rvert$	4.50^o	11.70^o	2.60
$\lvert\xi_{min}\rvert/\lvert\xi_{max}\rvert$	0.24	0.21	

The table shows that the mean yaw level of the 35mm firings is much higher than that of the 105mm case; however, the ratio of the minimum to maximum yaw is nearly equal for each. This is taken to indicate that the sabot discard interference has the same relative influence on the launch dynamics of the two rounds. The launch environment of the 35mm projectile is quantitatively more severe. The last row indicates that the launch impulses exerted upon the 35mm projectile are roughly three times greater than those exerted upon the 105mm projectile. Obviously, this factor of three is also the scale factor in the current replica modeling. Comparison of the measured

dispersion on target also produces this factor of three, Figure 15.

The level of yaw and large dispersion of the 35mm replica model indicates that exact, quantitative reproduction of the 105mm launch environment was not reproduced. One reason may be the difficulty in maintaining machining tolerances as the projectile is scaled down. Failure to scale any asymmetries due to these tolerances could produce a factor of three amplification of the vibration level in response to the higher, in-bore acceleration of the 35mm round. Another possible source of error is the difference between the gun mounts used in the current tests and in actual tank gun firings. The present set-up made use of an existing 37mm gun mount and sleigh. The tank gun recoil system is in no way similar. Even with this failure to achieve full replication of the tank gun performance, the tests demonstrate that the gross features of the launch dynamics are accurately reproduced and, further, that the measured details of the sabot discard process provide information which documents the interaction processes occurring.

IV. CONCLUSIONS

An experimental program has been conducted to examine the possibility of replica modeling of the launch and flight dynamics of complex, sabot, kinetic energy projectiles. The program acquired data on the interior ballistics, muzzle blast, sabot discard dynamics, and exterior ballistics of a one-third scale model of the 105mm, M68 tank gun firing the M392, sabot, spin-stabilized projectile. Comparison with full-scale test results shows good agreement between the interior ballistics, muzzle blast, and exterior ballistics of the two systems. The sabot discard and launch dynamics are shown to produce good qualitative correspondence; however, significant quantitative differences in the launch impulse levels are observed. The data on sabot discard produced good agreement with analytical treatment of the process and showed that the discard is inherently asymmetric.

ACKNOWLEDGEMENT

The authors wish to recognize the work of Messrs. D. D. Shear, W. Thompson, and D. McClellan without which the experiments could not have been conducted. The fine efforts of personnel involved in the manufacturing aspects of the program are greatly appreciated.

Figure 1a. Photograph of test projectiles

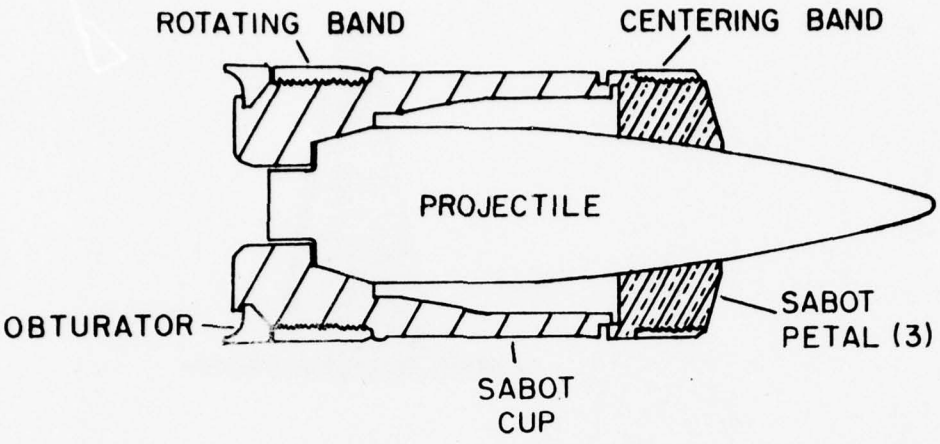

Figure 1b. Schematic of test projectiles

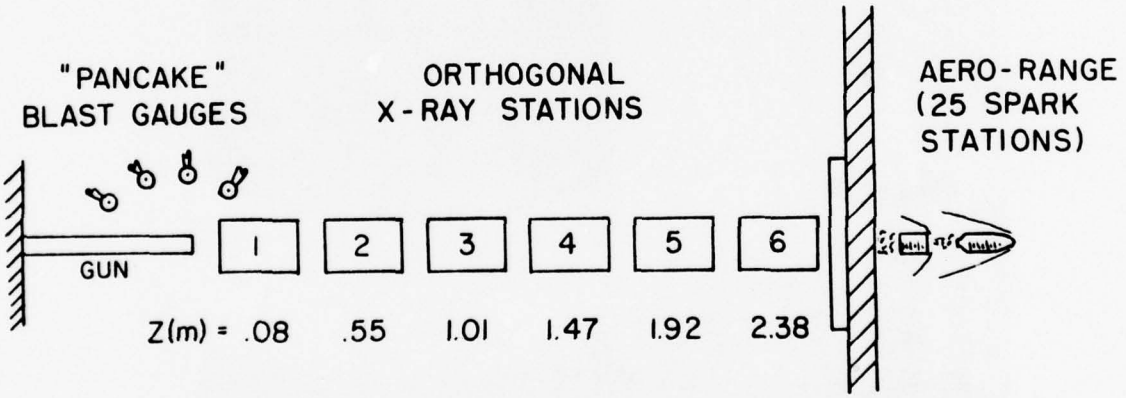

Figure 2. Test set-up in Aeroballistics Range

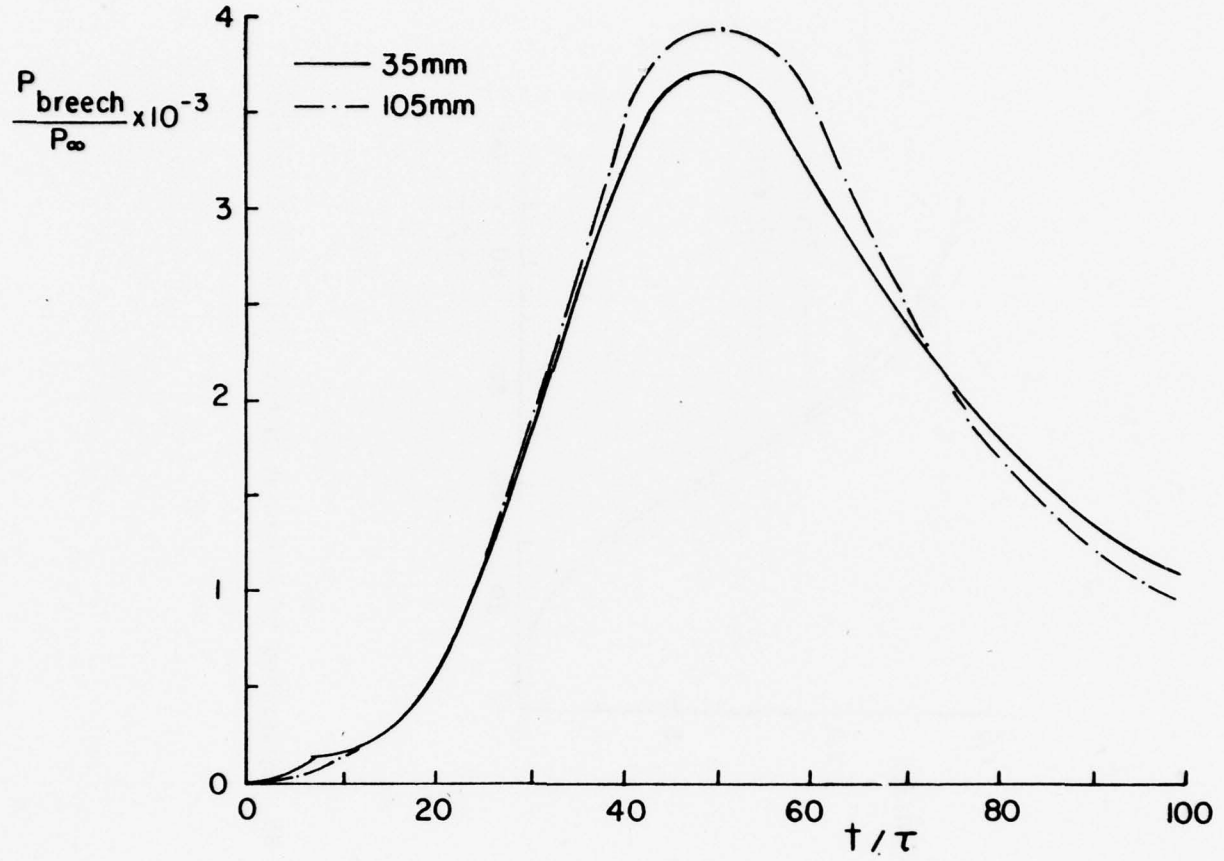

Figure 3a. Comparison of measured breech pressures

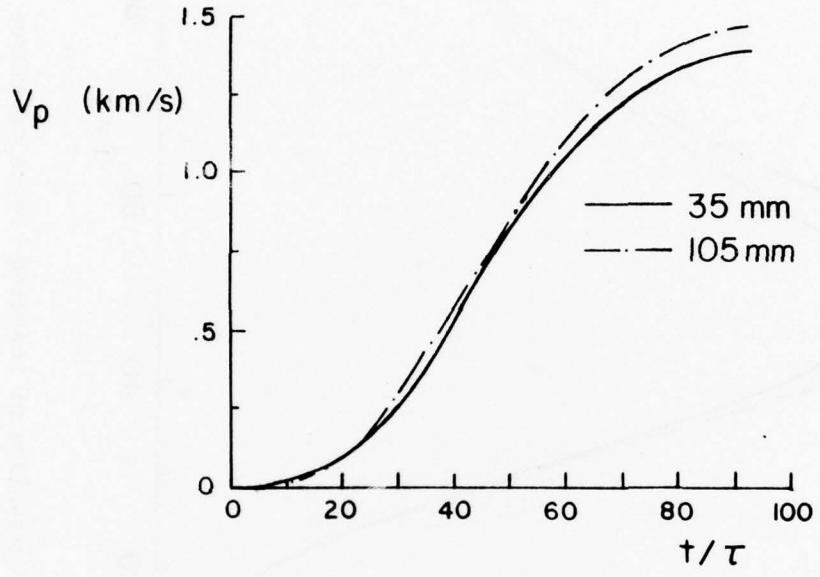

Figure 3b. Comparison of measured in-bore velocity histories

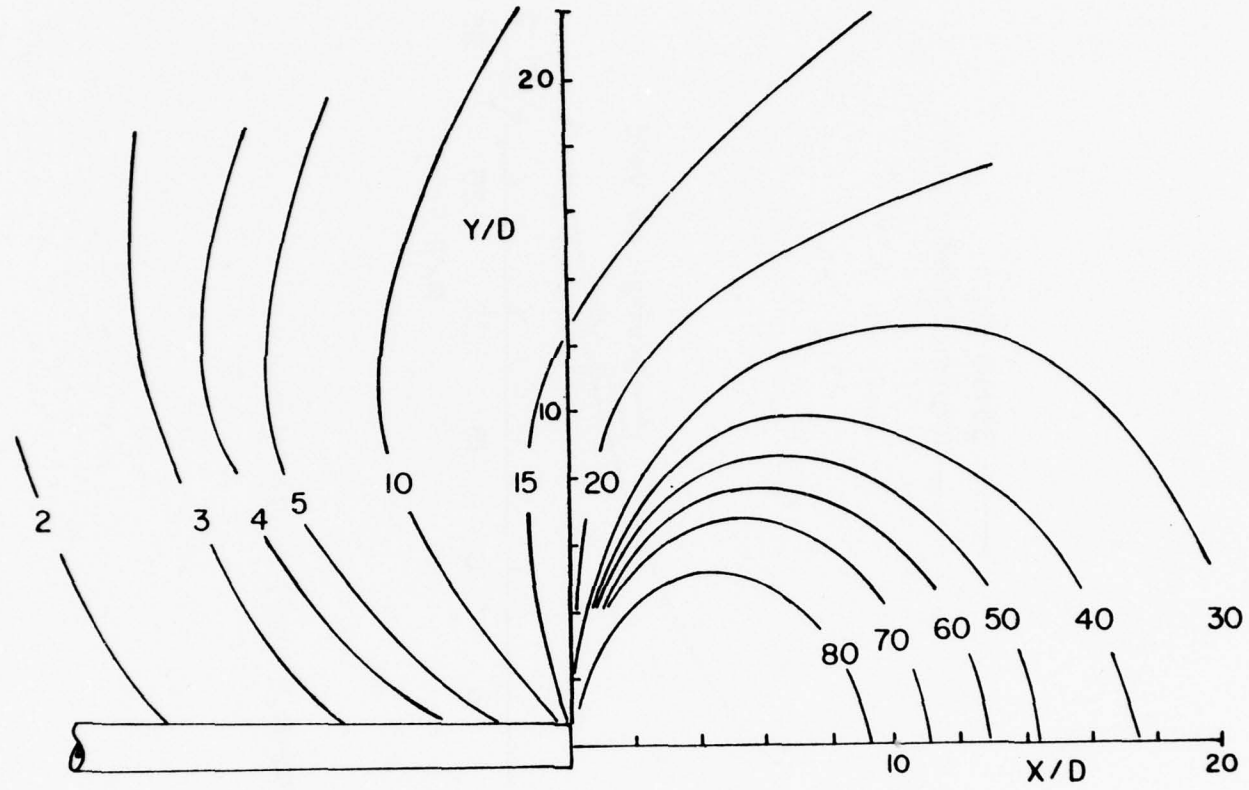

Figure 4. Measured blast overpressure contours (in psi) for the 35 mm gun

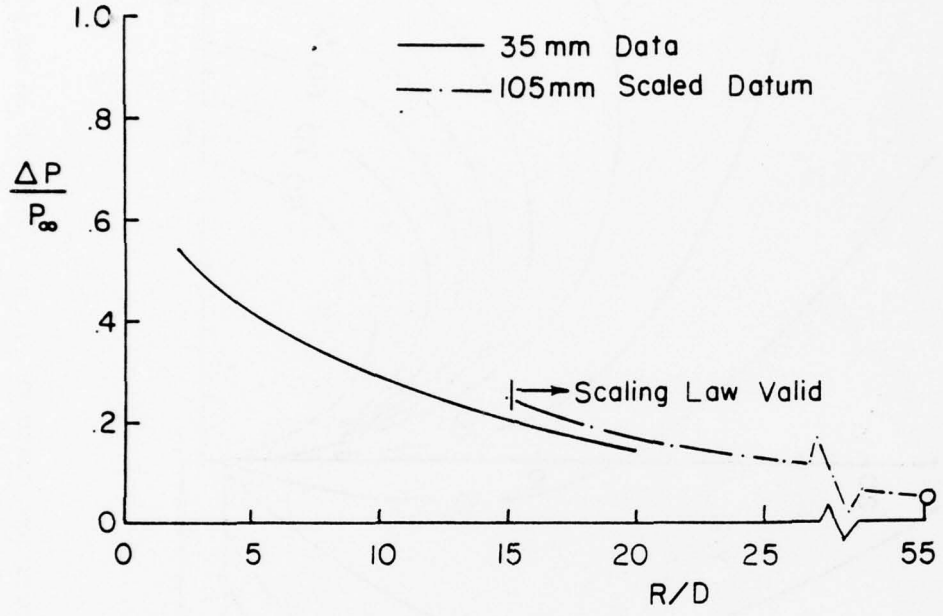

Figure 5. Overpressure correlation

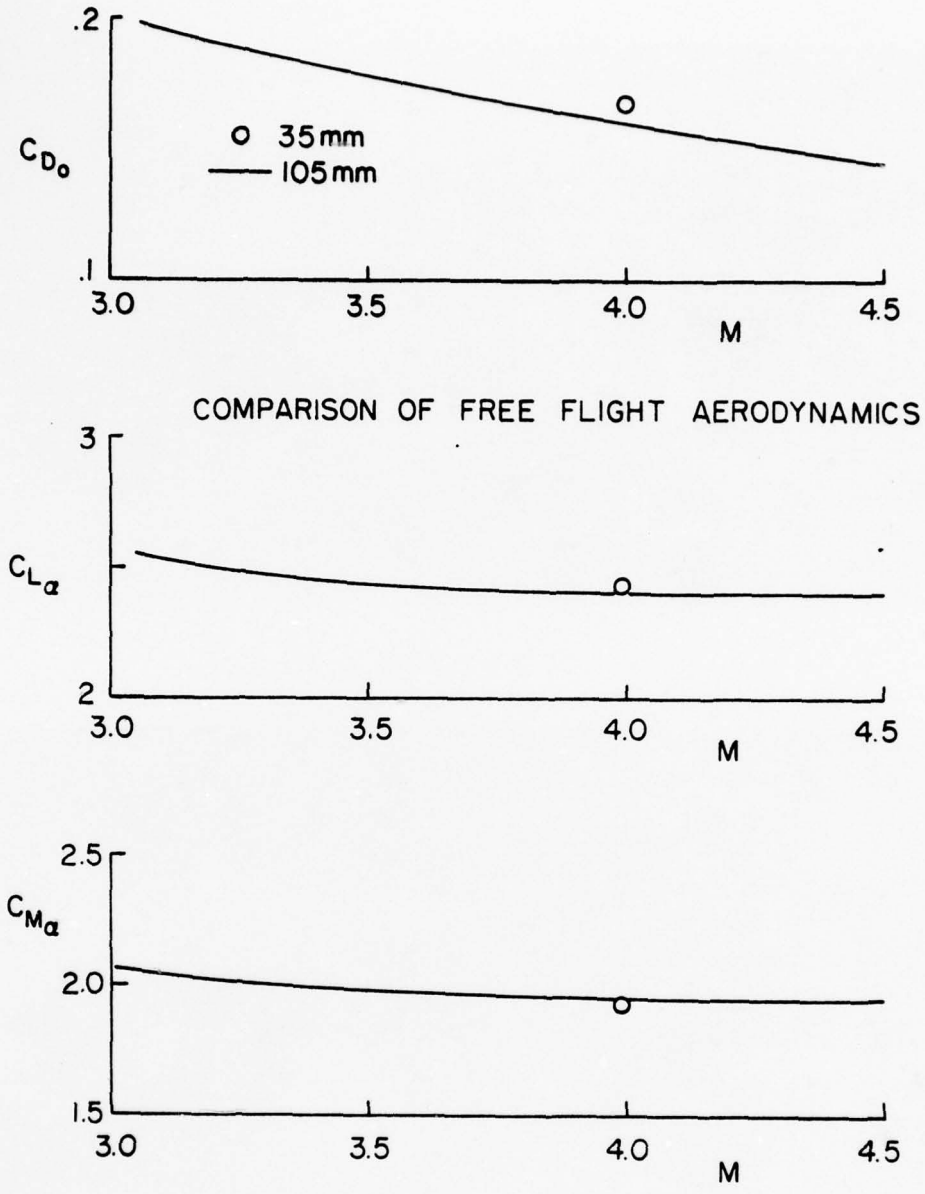

Figure 6. Comparison of aerodynamic coefficients

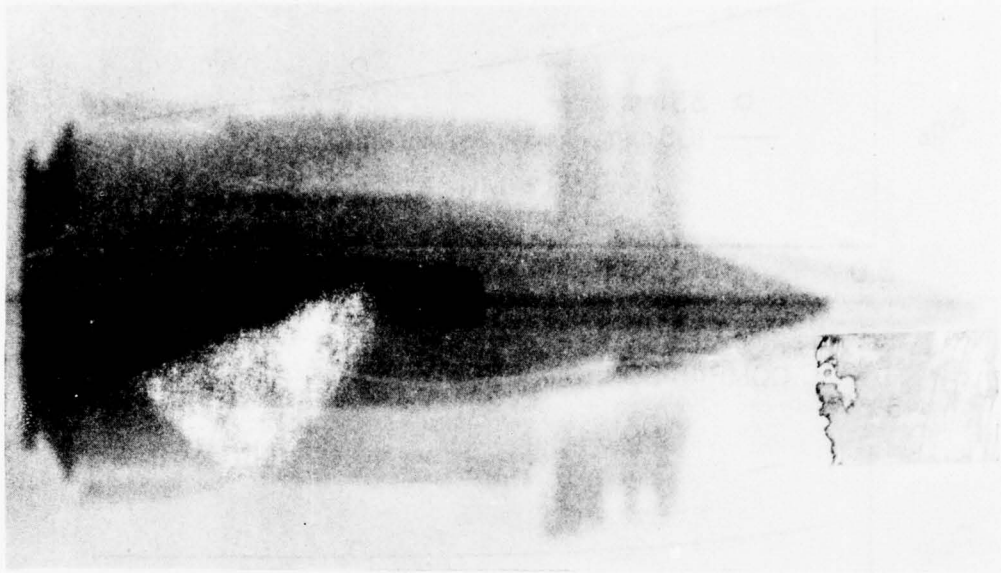

a. Z = 0.08 m

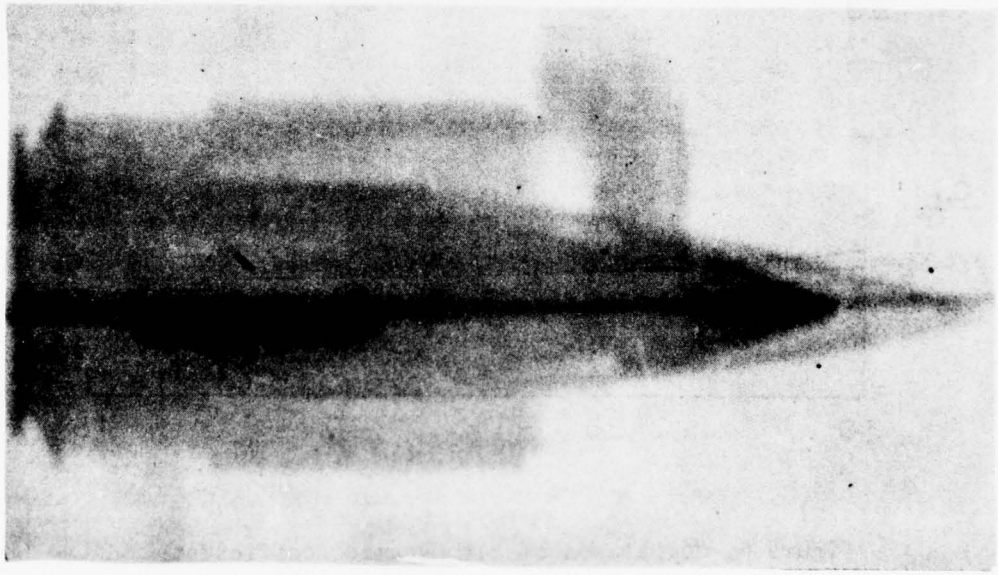

b. Z = 0.55 m

Figure 7. Sample sequence of X-ray photographs for 35 mm projectile

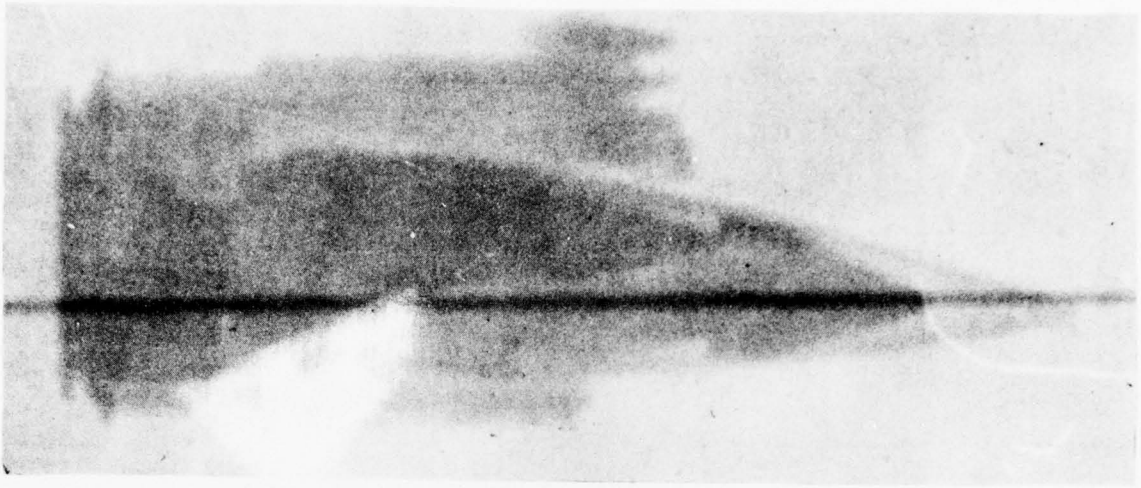

c. Z = 1.01 m

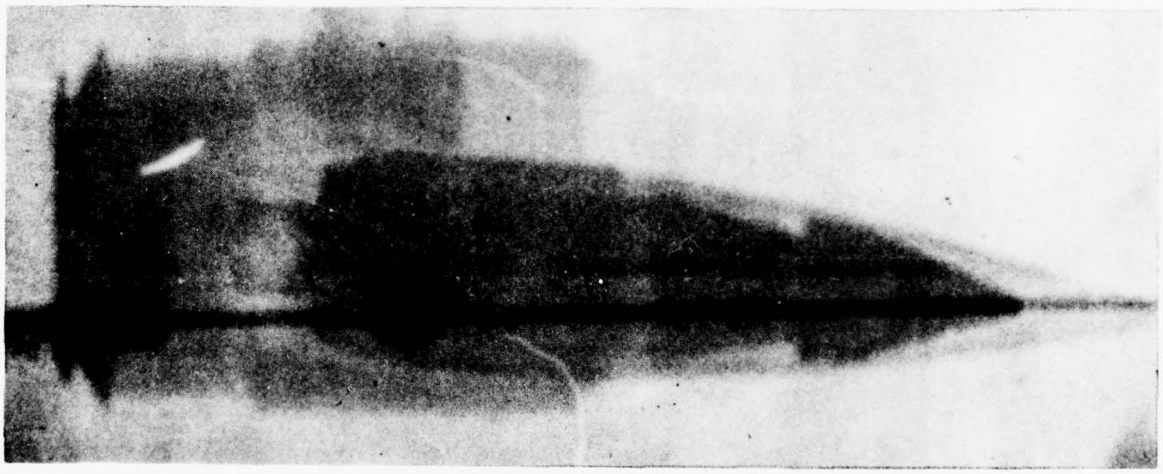

d. Z = 1.47 m

Figure 7. Sample sequence of X-ray photographs for 35 mm projectile

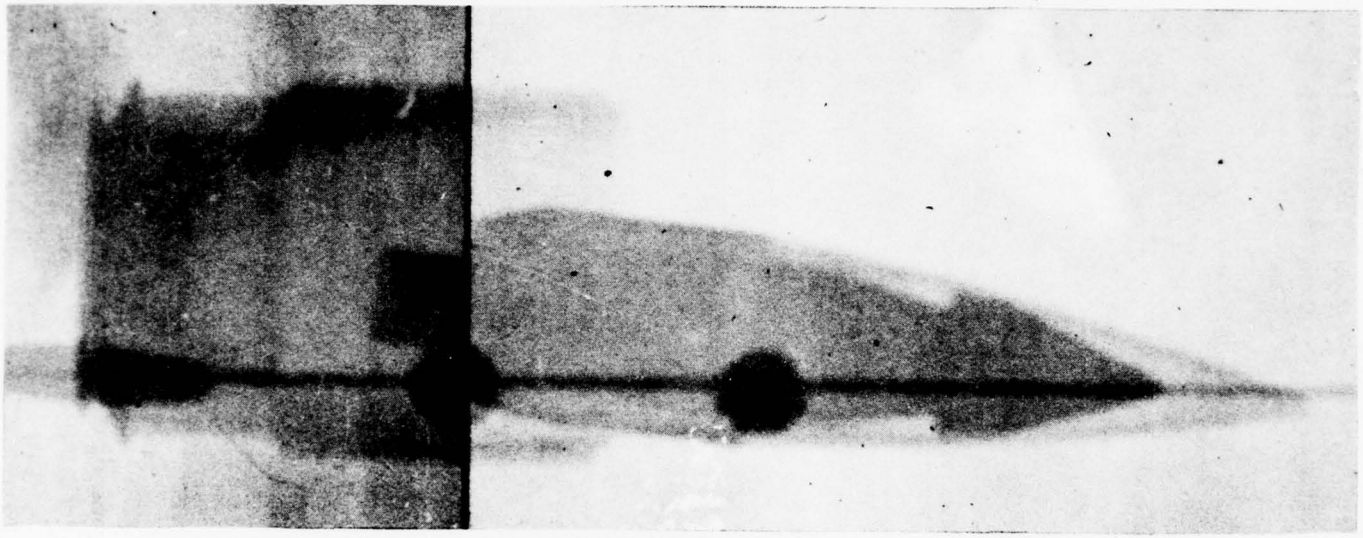

e. Z = 1.92 m

Figure 7. Sample sequence of X-ray photographs for 35 mm projectile

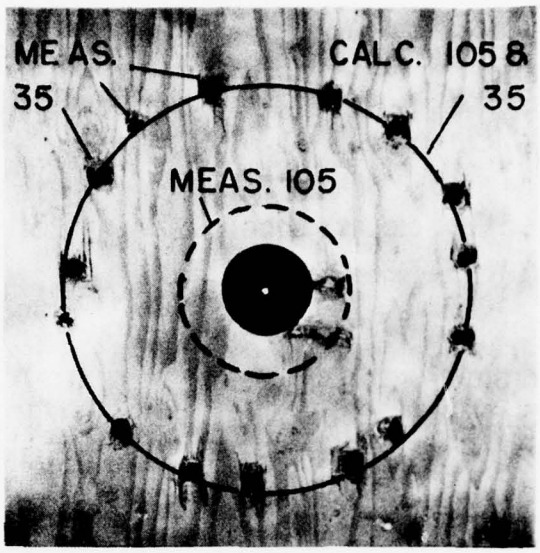

Figure 8. Sabot petal impacts on witness board

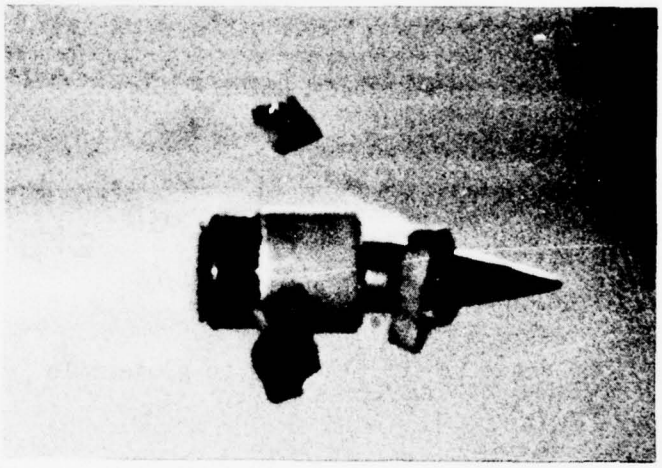

Figure 9. Smear photograph of 105 mm projectile, Z = 7.62 m

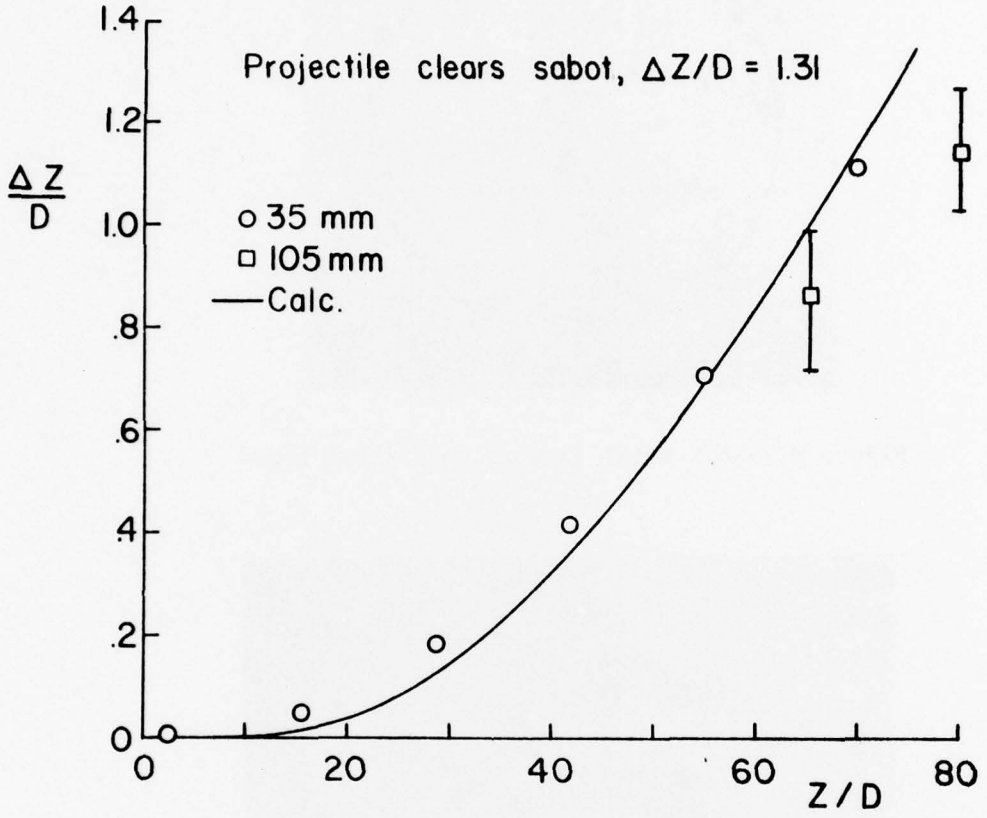

Figure 10. Sabot cup deceleration relative to projectile

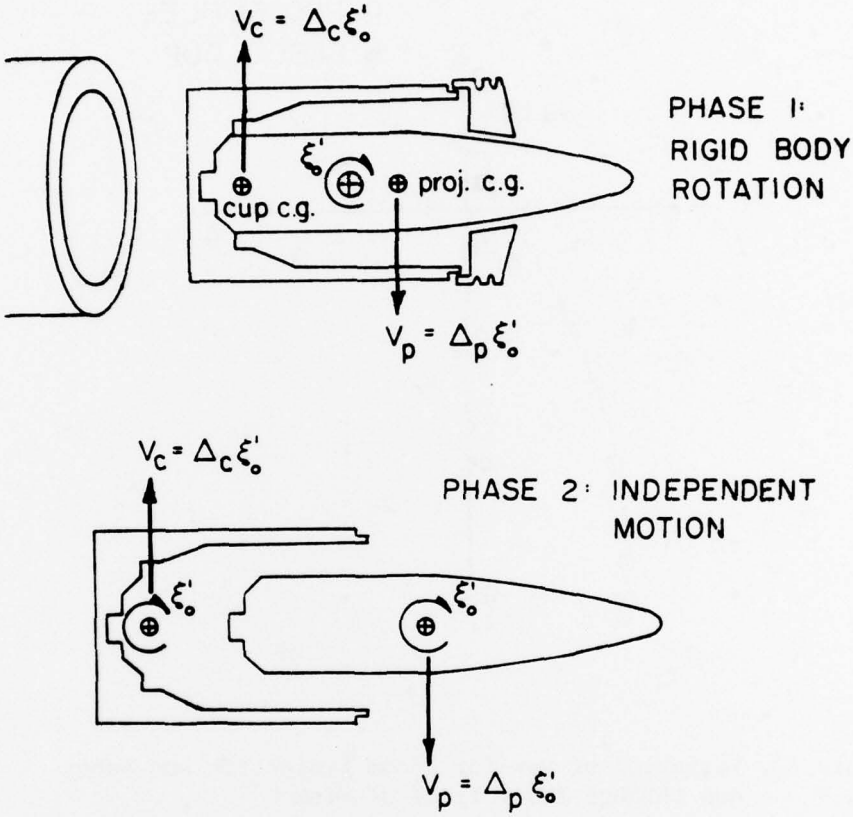

Figure 11. Model of sabot discard dynamics

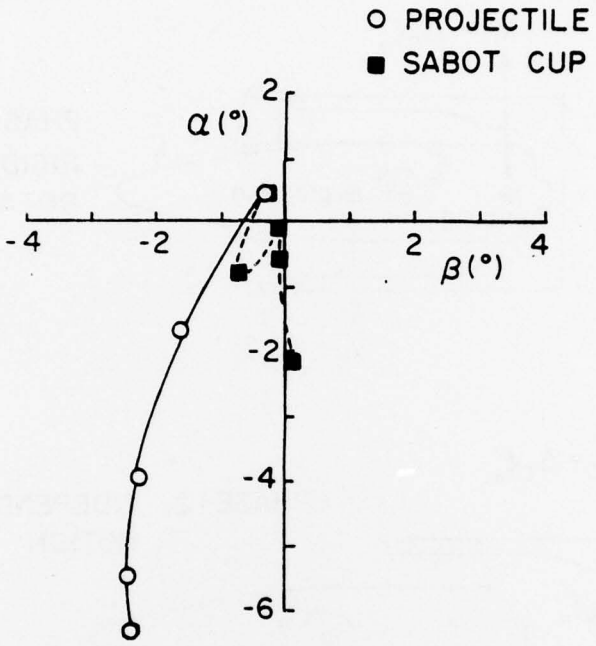

Figure 12. Variation of yaw for 35 mm projectile and sabot cup through X-ray field of view

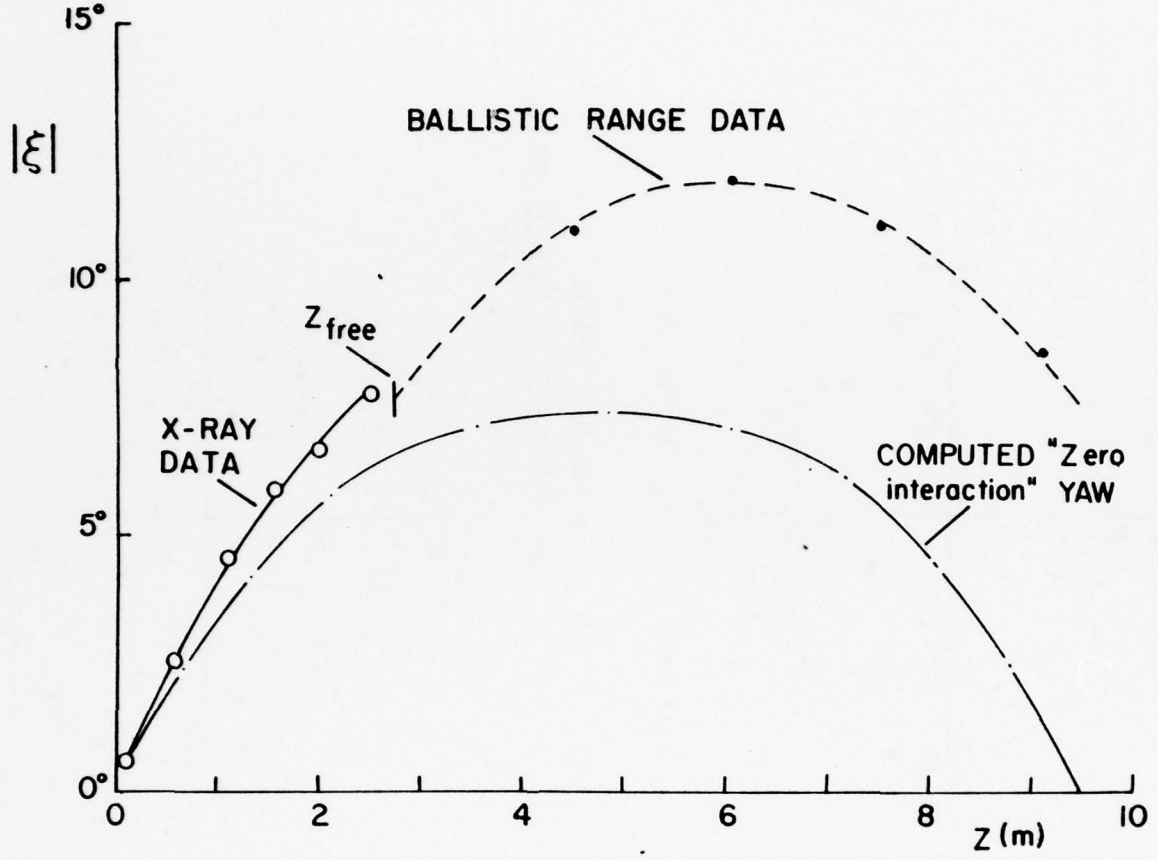

Figure 13. Variation in magnitude of yaw of 35 mm projectile as it moves downrange

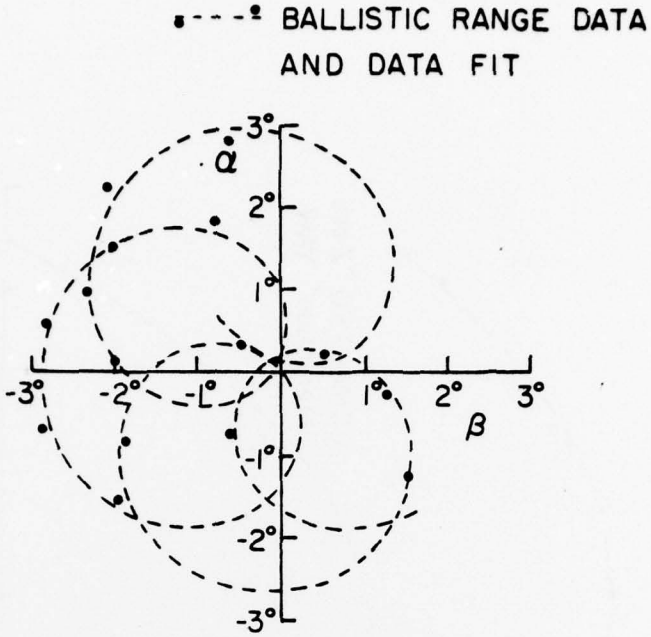

a. Full bore 175 mm projectile, M437

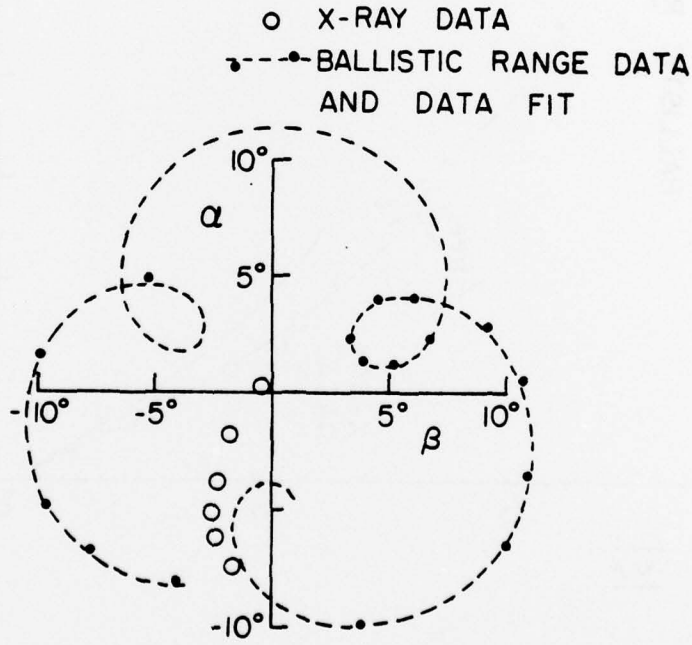

b. Subcaliber 35 mm projectile, M392

Figure 14. Measured yawing motions

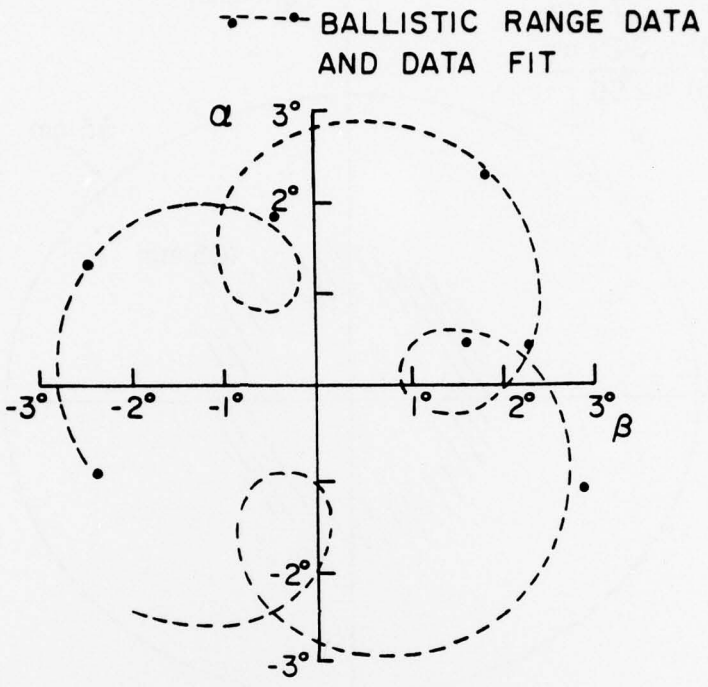

c. Subcaliber 105 mm projectile, M392

Figure 14. Measured yawing motions

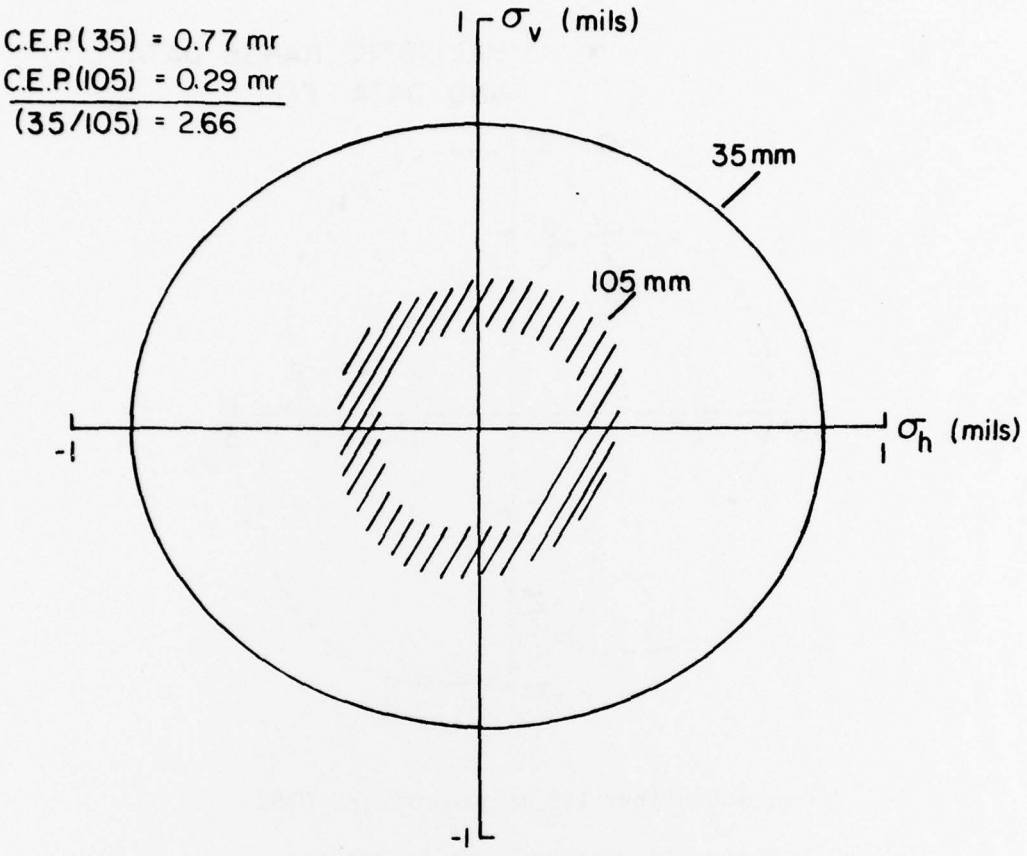

Figure 15. Comparison of measured impacts

REFERENCES

1. C. H. Murphy, "Free Flight Motion of Symmetric Missiles," U. S. Army Ballistic Research Laboratory Report No. 1216, July 1963, AD 442757.

2. F. Hunt, G. Hinds, C. Clemmow, and C. Tranter, (ed), Internal Ballistics, The Philosophical Library, New York, 1951.

3. J. M. Frankle, "Interior Ballistics of High-Velocity Guns, Experimental Program-Phase 1," BRL MR 1879, Ballistic Research Laboratory, Aberdeen Proving Ground, MD, November 1967. AD 830408.

4. E. Kelly, "Firing Record: Cartridge, 105mm, APDS-T, M392A2," FR P-82598, Test and Evaluation Command, Aberdeen Proving Ground, MD, June 1977.

5. M. Piddington and F. Brandon, Private Communication, Ballistic Research Laboratory, Aberdeen Proving Ground, MD, April 1978.

6. G. Samos, B. B. Grollman, and J. Q. Schmidt, "Initial Firing Test Results of the 35mm Scaled Model of the 105mm M68 Tank Gun," ARBRL MR 02804, Ballistic Research Laboratory, Aberdeen Proving Ground, MD, January 1978. AD A051050.

7. P. S. Westine, "The Blast Field About the Muzzle of Guns," Shock and Vibration Bulletin, No. 39, Pt. 6, March 1969.

8. E. M. Schmidt and E. J. Gion, "Muzzle Blast of 30mm Cannon," ARBRL-MR-02805, Ballistic Research Laboratory, Aberdeen Proving Ground, MD, January 1978. AD B024973L.

9. J. Ranlet and J. Erdos, "Muzzle Blast Field Calculations," CR 297, Ballistic Research Laboratory, Aberdeen Proving Ground, MD, April 1976. AD B011967L.

10. E. M. Schmidt, K. S. Fansler, and D. D. Shear, "Trajectory Perturbations of Fin-Stabilized Projectiles due to Muzzle Blast," AIAA, JSR, Vol. 14, No. 6, June 1977, pp. 339-344.

LIST OF SYMBOLS

C_D, C_{L_α}, C_{M_α}	drag, lift, and moment coefficient
D	diameter of gun tube
e_c	propellant specific energy
I_x, I_y	axial and transverse moments of inertia
L	length of gun tube
ℓ	diameter of flight body
M	moment
m	mass
p	pressure (side-on)
r	radial distance from gun muzzle
s_g	gyroscopic stability factor
T	period of yaw in meters
V_m	muzzle velocity
Z	downrange displacement (Z = 0 at muzzle)
γ	ratio of specific heats
ξ	complex angle of yaw, $\beta + i\alpha$
ρ	density
τ	D/V_m, reference time
Φ_o'	launch spin (radians/caliber)

DISTRIBUTION LIST

No. of Copies	Organization
12	Commander Defense Documentation Center ATTN: DDC-TCA Cameron Station Alexandria, VA 22314
1	Director Defense Nuclear Agency Washington, DC 20305
1	Commander US Army Materiel Development and Readiness Command ATTN: DRCDMD-ST, N. Klein 5001 Eisenhower Avenue Alexandria, VA 22333
1	Commander US Army Materiel Development and Readiness Command ATTN: DRCDL 5001 Eisenhower Avenue Alexandria, VA 22333
1	Commander US ARmy Aviation Research and Development Command ATTN: DRSAV-E P. O. Box 209 St. Louis, MO 63166
1	Director US Army Air Mobility Research and Development Laboratory Ames Research Center Moffett Field, CA 94035
1	Commander US Army Electronics Research and Development Command Technical Support Activity ATTN: DELSD-L Fort Monmouth, NJ 07703
1	Commander US Army Jefferson Proving Ground ATTN: STEJP-TD-D Madison, IN 47250
1	Commander US Army Communications Rsch and Development Command ATTN: DRDCO-SGS Fort Monmouth, NJ 07703
1	Commander US Army Missile Materiel Readiness Command ATTN: DRSMI-AOM Redstone Arsenal, AL 35809
3	Commander US Army Missile Research and Development Command ATTN: DRDMI-R DRDMI-RBL DRDMI-RDK Redstone Arsenal, AL 35809
1	Commander US Army Tank Automotive Research & Development Cmd ATTN: DRDTA-UL Warren, MI 48090
1	Commander US Army Armament Materiel Readiness Command ATTN: DRSAR-LEP-L, Tech Lib Rock Island, IL 61299
6	Commander US Army Armament Research and Development Command ATTN: DRDAR-TSS (2 cys) DRDAR-TDS, Mr. Lindner DRDAR-TDA, Mr. Blick DRDAR-LC-F, Mr. A. Loeb Mr. E. Friedman Dover, NJ 07801

DISTRIBUTION LIST

No. of Copies	Organization
7	Commander US Army Armament Research and Development Command ATTN: DRDAR-LCV, Mr. Barrieres Mr. Reisman DRDAR-SCN, Mr. Kahn DRDAR-SCW, Mr. Townsend DRDAR-SC (Dr. T. Hung) PM, XM788/789, LTC Delany Dover, NJ 07801
6	Commander US Army Watervliet Arsenal ATTN: DRDAR-LCB-TL Mr. W. Dock Dr. G. Carofano Mr. P. Alto DRDAR-LCB, Mr. T. Allen Mr. R. Billington Watervliet, NY 12189
1	Commander US Army Materials and Mechanics Research Center ATTN: DRXMR-ATL Watertown, MA 02172
1	Commander US Army Natick Research and Development Command ATTN: DRXRE, Dr. D. Sieling Natick, MA 01762
2	Director US Army TRADOC Systems Analysis Activity ATTN: ATAA-SL, Tech Lib ATAA-S White Sands Missile Range NM 88002
1	Commander US Army Research Office ATTN: CRD-AA-EH P. O. Box 12211 Research Triangle Park NC 27709
1	Director US Army BMD Advanced Technology Center P.O. Box 1500, West Station Huntsville, AL 35807
1	Commander US Army Ballistic Missile Defense Systems Command Huntsville, AL 35804
3	Commander Naval Air Systems Command ATTN: AIR-604 Washington, DC 20360
3	Commander Naval Ordnance Systems Cmd ATTN: ORD-9132 Washington, DC 20360
2	Commander and Director David W. Taylor Naval Ship Research & Development Cmd ATTN: Lib Div, Code 522 Aerodynamic Lab Bethesda, MD 20084
3	Commander Naval Surface Weapons Center ATTN: Code 6X Mr. F. H. Maille Dr. J. Yagla Dr. G. Moore Dahlgren, VA 22448
1	Commander Naval Surface Weapons Center ATTN: Code 730, Tech Lib Silver Spring, MD 20910
1	Commander Naval Weapons Center ATTN: Code 553, Tech Lib China Lake, CA 93555

DISTRIBUTION LIST

No. of Copies	Organization
1	Commander Naval Research Laboratory ATTN: Tech Info Div Washington, DC 20375
1	Commander Naval Ordnance Station ATTN: Code FS13A, P. Sewell Indian Head, MD 20640
1	AFRPL/LKCB, Dr. Horning Edwards AFB, CA 93523
2	AFATL (DLRA, F. Burgess; Tech Lib) Eglin AFB, FL 32542
1	AFWL/DEV Kirtland AFB, NM 87117
1	ASD/XRA (Stinfo) Wright-Patterson AFB, OH 45433
1	Director National Aeronautics and Space Administration George C. Marshall Space Flight Center ATTN: MS-I, Lib Huntsville, AL 38512
1	Director Jet Propulsion Laboratory ATTN: Tech Lib 2800 Oak Grove Drive Pasadena, CA 91103
1	Director National Aeronautics and Space Administration Langley Research Center ATTN: MS 185, Tech Lib Langley Station Hampton, VA 23365
1	Director NASA Scientific & Technical Information Facility ATTN: SAK/DL P. O. Box 8757 Baltimore/Washington International Airport, MD 21240
1	AAI Corporation ATTN: Dr. T. Stastny Cockeysville, MD 21030
1	Advanced Technology Labs ATTN: Mr. J. Ranlet Merrick & Steward Avenues Westbury, NY 11590
1	Aerospace Corporation ATTN: Dr. T. Taylor P. O. Box 92957 Los Angeles, CA 90009
1	ARO, Inc. ATTN: Tech Lib Arnold AFS, TN 37389
1	ARO, Inc. Von Karman Gasdynamics Facility ATTN: Dr. J. Adams Arnold AFS, TN 37389
1	ARTEC Associates, Inc. ATTN: Dr. S. Gill 26046 Eden Landing Road Hayward, CA 94545
1	AVCO Systems Division ATTN: Dr. W. Reinecke 201 Lowell Street Wilmington, MA 01887
1	Battelle Columbus Laboratories ATTN: J. E. Backofen, Jr. 505 King Avenue Columbus, OH 43201

DISTRIBUTION LIST

No. of Copies	Organization
1	Technical Director Colt Firearms Corporation 150 Huyshope Avenue Hartford, CT 14061
2	General Electric Corporation Armaments Division ATTN: Mr. R. Whyte Mr. J. MacNeil Lakeside Avenue Burlington, VT 05401
1	Honeywell, Inc. ATTN: Mail Station MN 112190 (G. Stilley) 600 Second Street, North Hopkins, MN 55343
1	Martin Marietta Aerospace ATTN: Mr. A. J. Culotta P. O. Box 5387 Orlando, FL 32805
1	Winchester-Western Division Olin Corporation New Haven, CT 06504
1	Rockwell Int'l Science Center ATTN: Dr. Norman Malmuth P. O. Box 1085 1000 Oaks, CA 91360
1	Sandia Laboratories ATTN: Aerodynamics Dept Org 5620, R. Maydew Albuquerque, NM 87115
1	S&D Dynamics, Inc. ATTN: Dr. M. Soifer 755 New York Avenue Huntington, NY 11743
1	Guggenheim Aeronautical Lab California Institute of Tech ATTN: Tech Lib Pasadena, CA 91104
1	Franklin Institute ATTN: Tech Lib Race & 20th Streets Philadelphia, PA 19103
1	Director Applied Physics Laboratory The Johns Hopkins University Johns Hopkins Road Laurel, MD 20810
1	Massachusetts Institute of Technology Dept of Aeronautics and Astronautics ATTN: Tech Lib 77 Massachusetts Avenue Cambridge, MA 02139
1	Ohio State University Dept of Aeronautics and Astronautical Engineering ATTN: Tech Lib Columbus, OH 43210
2	Polytechnic Institute of New York Graduate Center ATTN: Tech Lib Dr. G. Moretti Route 110 Farmingdale, NY 11735
1	Director Forrestal Research Center Princeton University Princeton, NJ 08540
1	Southwest Research Institute ATTN: Mr. Peter S. Westine P. O. Drawer 28510 8500 Culebra Road San Antonio, TX 78228

DISTRIBUTION LIST

Aberdeen Proving Ground

Dir, USAMSAA
Cdr, USATECOM
ATTN: DRSTE-SG-H
Cdr, USA CSL/EA
ATTN: A. Flatau, SAREA-DE-W
Bldg. E3516